Ficus religiosa Fruits-mediated Synthesis of CeO_2 Nanoparticles and CeO_2/CuO Nanocomposites: Structural Insights and Antimicrobial Efficacy

Mohammed K. Nagshabandi,[a] Samy Selim ,[b,*] Mohammed H. Alruhaili,[c,e] Hattan S. Gattan,[d,e] , Tarek M. Abdelghany ,[f] and Mohamed A. Amin ,[f,*]

A novel, simple, and inexpensive technique, chemical coprecipitation, was employed to produce CeO_2 nanoparticles and CeO_2/CuO nanocomposite. It entailed reacting dehydrated metal nitrate salts with an aqueous extract of *Ficus religiosa*. The CeO_2 and CeO_2/CuO solids were identified by X-ray diffraction (XRD), FTIR, and transmission electron microscopy (TEM). The diffraction peaks of the CeO_2 and CeO_2/CuO revealed cubic and monoclinic structures, respectively, with average crystallite sizes of 20.5 and 26.8 nm, based on the XRD data. TEM examinations show that the mean sizes of CeO_2 and CeO_2/CuO particles were (39.8 and 66.5 nm, respectively). These results imply negligible agglomeration. This study evaluated the antimicrobial efficacy of CeO_2/CuO nanocomposite and CeO_2/CuO NPs against bacterial and fungal pathogens. The nanocomposite exhibited superior activity, producing larger inhibition zones (*Bacillus subtilis*: 26 mm; *Candida albicans*: 28 mm) compared to CeO_2 NPs and the standard drugs ciprofloxacin (as antibiotic) and nystatin (as antifungal). MIC and MBC/MFC assays confirmed stronger potency, particularly against Gram-positive bacteria and *C. albicans*. Time–kill kinetics revealed complete eradication of *B. subtilis* and *K. pneumoniae* within 180 min, while partial survival occurred in *S. aureus* and *S. typhi*. Both materials were inactive against *Aspergillus niger*, indicating selective but potent antimicrobial effects.

DOI: 10.15376/biores.21.1.1224-1237

Keywords: Green synthesis; Pathogen control; CeO_2/CuO; Nanocomposites

Contact information a: Department of Basic Medical Sciences, College of Medicine, University of Jeddah, Jeddah, Saudi Arabia; b: Department of Clinical Laboratory Sciences, College of Applied Medical Sciences, Jouf University, Sakaka, Saudi Arabia; c: Department of Clinical Microbiology and Immunology, Faculty of Medicine, King Abdulaziz University, 21589, Jeddah, Saudi Arabia; d: Department of Medical Laboratory Sciences, Faculty of Applied Medical Sciences, King Abdulaziz University, Jeddah, Saudi Arabia; e: Special Infectious Agents Unit, King Fahad Medical Research center, King Abdulaziz University, Jeddah, Saudi Arabia; f: Botany and Microbiology Department, Faculty of Science (Boys), Al-Azhar University, Cairo 11884, Egypt;
** Corresponding authors: sabdulsalam@ju.edu.sa; mamin7780@azhar.edu.eg*

INTRODUCTION

New methods regarding multidrug-resistant bacteria and cancer cells and increasing the effectiveness of treatment can be provided by nanotechnology (Jelonek *et al*. 2018). Recent studies have revealed the active function of CeO nanoparticles (NPs) as an anticancer agent (Lu, *et al* 2022; Abbasi, *et al* 2022; Al-Attar *et al*. 2025). CeO_2 nanoparticles (NPs) are suitable and more and more prevalent in biological utilizations due

to their intrinsic properties, which include reverse electrical state since Ce(III) shifts to Ce (IV) and oxidation-reduction activity triggered by interface vacancies in oxygen. This enables them to scavenge reactive oxygen species (ROS) (Sadidi *et al*. 2020). General particle size reduction to nanoscale levels in nanomaterials can have major effect on activities (Abdelghany 2013; Abdelghany *et al*. 2018; Al-Rajhi *et al*. 2022a; Amin *et al*. 2024, 2025; Soliman *et al*. 2024; Selim *et al*. 2025a, 2025b).

With the increasing use of synthesis techniques that control final form and size, nanoparticles now offer tremendous potential, especially for medical applications (Amiri *et al*. 2021; Al-Rajhi *et al*. 2022b; Alghonaim *et al*. 2024; Alghonaim *et al*. 2025). CeO_2 NPs are employed in a extensive range of biomedical scientific fields, involving catalytic processes, gas detection, and in optical devices (Nadeem *et al*. 2020). Aseyd Nezhad *et al.* (2020) reported that CeO_2-NP were created by utilizing leaf extract from *Origanum majorana* L. The biocreated CeO_2-NP verified antioxidant efficacy *via* scavenging free radicals from DPPH and ABTS. Therefore, the greater effects of CeO_2-NP on cancer of breast cell lines as opposed to non-cancer cells suggested that this NP might be used as an anti-cancer drug (Aseyd Nezhad *et al*. 2020). CeO_2 nano-decorated with copper (Cu/CeO_2), at 100 mg/L dose, was found to have a 100% free radical scavenging action, with the same level of activity as the reference substances ascorbic acid and Trolox at 50 mg/L (Şener *et al.* 2024). The pure cubic crystalline form with a face fluorite structure of CeO_2 NPs, which were made from *Cassia glauca* flower aqueous extract and had a mean diameter of 3.20 nm, showed poor to moderate efficiency against several types of bacteria in another investigation (Butt *et al*. 2022). When compared to Gram-positive bacteria, the naturally produced CeO_2 NPs show significant antibacterial action as mentioned by Sarita Rai *et al.* (2024) contrary to *Pseudomonas aeruginosa* and *Escherichia coli.* Furthermore, the goal of the deliberate dual doping of copper and cerium is to enhance CuO NPs' functional potential and biocompatibility; this idea has not been thoroughly reported in the literature. This duple-functionalization style suggests a capable new path toward the development of multifunctional nanomaterials with improved beneficial efficacy. Therefore, this study's goal was to investigate how *Ficus religiosa* extract produced CeO_2 and CeO_2/CuO NPs for the first time. This is study is novel in that the generated NPs were assessed for their antibacterial qualities to fight resistant microorganisms.

EXPERIMENTAL

Material

Sigma Aldrich supplied 99.5% pure cerium nitrate ($Ce(NO_3)_2{\cdot}6H_2O$) and copper nitrate ($Cu(NO_3)_2{\cdot}3H_2O$), among other common chemicals.

Methods

Biogenic creation of cerium oxide nanoparticles

Cerium oxide NPs were synthesized using a modified version of the published methodology (Naz *et al*. 2019) using *Ficus religiosa* fruit extract. A light-red solution was produced by boiling ten g of the fruits (air dried) per 500 mL of distilled water for 10 min. A clear extract was then obtained by cooling and filtering the mixture. Then 100 mL of fruit extract at pH 9 was added to 2.5 g of cerium nitrate salt. For 3 h, the reaction was agitated at 1000 rpm and 75±5 °C. After centrifuging at 8000 g for 10 min, the NPs were

recovered and given three washes with distilled water. At 400 °C, the NPs were calcined for two hours.

Biogenic creation of cerium oxide/copper oxide nanoparticles

Copper nitrate (0.3M) with (0.7M) cerium nitrate were mixed independently in 50 mL of fruit extract, beside urea (100 mL) was gradually mixed with the binary solution while being stirred for an hour. The solution was treated with sodium hydroxide drop by drop until the pH reached to10 at 60 ℃. After the suspension was separated by centrifugation and rinsed with distilled water and ethanol, it was dried in an oven set at 100 °C for six hours. At 600 °C, the powder was calcined for 2 h. The dual nanocomposite (dark brown precipitate) was produced as a result (Salih *et al*. 2024).

Description of CeO_2 and CuO Nanocomposites

TEM (TEM, model JEOLJEM-2100, manufactured in Japan) was used to study size and morphology. X-ray diffraction was employed to determine the crystallinity structure (Philips PW17320). The Scherrer's equation, $D = K\lambda/\beta\cos\theta$, was employed to calculate the crystalline dimensions of NPs. D is the crystallite size, λ is the CuKα wavelength (1.5 Aº), θ is the diffraction angle, and β is the full width at half maximum (FWHM) of the diffraction peaks (in radians). FTIR spectroscopy of NPs was achieved via Nicolet TM380 to determine the functional groups of biomolecules enclosed on their surface.

The stability and hydrodynamic diameter of NPs in an aqueous medium were examined via the DLS technique. Zeta-potential was measured at 20±1°C using a semiconductor laser (40 mW, λ = 658 nm) using the Litesizer 500 photon linked to spectroscopy apparatus (Anton Paar GmbH, Austria).

Antimicrobial Activity (Well Diffusion) and MIC, MBC, and MFC Assays

The antibacterial potential of the created NPs was assessed via agar well diffusion approach, along with a standard antimicrobial agent ciprofloxacin (10 µg/mL, as antibiotic) and nystatin (100 µg/mL as antifungal) for comparison (Selim *et al*. 2025a). Mueller-Hinton agar (MHA) was used to cultivate fresh bacterial cultures of *Staphylococcus aureus* (ATCC 6538), *Bacillus subtilis* (ATCC 6633), *Salmonella typhi* (ATCC 6539), and *Klebsiella pneumoniae* (ATCC 13883) overnight at 37 °C, while other medium namely Sabouraud dextrose agar (SDA) was employed to propagate *Candida albicans* (ATCC 10221) and *Aspergillus niger* (ATCC 16888) at 28 to 30 °C). To create the microbial inoculum, freshly created colonies in sterile saline were suspended, and the turbidity was adapted to 0.5 McFarland standard (1 x 10^2 CFU/mL for bacteria). For fungi, suspensions of spores or yeast were made and adjusted to 10^{-10} CFU/mL.

To create a uniform lawn of growth, 100 µL of the microbial slurry was evenly injected onto each sterile agar plate using a sterile cotton cloth. A sterile cork borer was functioned to aseptically create wells with a width of 8 mm after the surface had been allowed to dry for a few minutes. Each test sample (CeO_2/CuO nanocomposite and CeO_2 NPs) was added to the corresponding well in a constant volume (50 µL). Sterile DMSO was utilized as a negative control.

Before incubation, the plates were allowed to properly diffuse for 30 to 60 min at room temperature. Fungal plates were incubated at 28 to 30 °C for 48 to 72 h, while bacterial plates were kept at 37 °C for 24 h. A digital caliper was used to measure the inhibition zone diameters in millimeters after incubation. Every experiment was carried

out in triplicate, and the results were reported as mean ± standard deviation. To ascertain relative inhibitory strength, the CeO_2/CuO nanocomposite's antibacterial efficacy was compared to that of CeO_2 NPs and conventional medications (Al Abboud *et al.* 2024). The broth microdilution technique was employed to calculate the minimum inhibitory concentration (MIC) values.

In sterile nutritional broth, serial two-fold dilutions ranging from 1000 to 7.8 µg/mL of each nanoparticles suspension were made. 100 µL of the standardized microbiological solution was mixed to each dilution, and it was then incubated at the proper temperature (37 °C for 24 h for bacteria, 30 °C for 48 to 72 h for fungus). The MIC was defined as the lowest concentration exhibiting no discernible turbidity. 100 µL solutions from tubes with no discernible growth were plated on fresh agar and cultured under the same conditions once again in order to calculate the MBC/MFC. The MBC or MFC was the lowest concentration that produced no colony growth on agar plates.

Killing Time (Time–Kill Kinetics) Assay

Using time-kill kinetics, the activity of CeO_2/CuO nanocomposite and CeO_2 NPs was evaluated. In short, overnight cultures of *S. aureus*, *K. pneumoniae*, *S. typhi*, and *B. subtilis* were adjusted to around 1×10^2 CFU/mL in sterile nutritional broth. The investigated substances were administered to aliquots at dosages that matched their corresponding minimum inhibitory concentrations. Samples were taken out of the bacterial suspensions at predefined intervals (0, 30, 60, 120, 150, and 180 minutes) while they were being gently shaken at 37 °C.

A serial dilution of 100 µL of the treated culture in sterile saline was applied to nutrient agar plates at each time point. Next a 24-h incubation time at 37 °C, the number of colonies that survived was measured in CFU/mL (Selim *et al*. 2024). A decrease in CFU with time relative to the original inoculum was used to describe the Time-Kill Kinetics effect.

Analytical Statistics

Minitab 18 was employed for statistical subtractions at 0.05, post hoc Tukey's assessment were utilized to study quantifiable data.

RESULTS AND DISCUSSION

The fruit extract from *Ficus religiosa* produced brown CeO_2 NPs and dark green of CeO_2/CuO nanocomposite. Various researchers have also documented similar color changes in CeO_2NPs manufactured using different techniques (Butt *et al*. 2022). Another crucial physical characteristic for biological applications is the shape of the nanoparticles. The shapes of the green synthesized CeO_2 and CeO_2/CuO NPs are shown in Figs. 1(a,d). Agglomeration of these NPs is apparent. Particle size decreased with increase in the likelihood of agglomeration. Because nanoparticles tend to minimize the exposed surface area to lower surface energy, agglomeration is a common behavior that occurs; hence, smaller particle sizes result in stronger agglomeration (Valsaraj and Divyarthana 2019). CeO_2 and CeO_2 /CuO NPs were revealed to be spherical and semispherical shapes, in the TEM images (Figs. 1a,d). The TEM images based on imagej program appeared that CeO_2 NPs and CeO_2/CuO nanocomposite have average size of (39.84 and 66.49 nm).

Additionally, the TEM picture reveals a thin film encircling the generated NPs, which could be a plant extract acting as a capping or protecting agent. These substances are believed to aid in protecting the produced nanoparticles. The average size of the aforementioned particle, as determined by DLS, was 42.1 nm for CeO_2 and 70.5 nm for CeO/CuO (Figs. 1c, 1f). The produced Se/Zn and Se/Zn/GB NPs showed a crystal-like appearance in the SAED pattern (Figs. 1b, 1e).

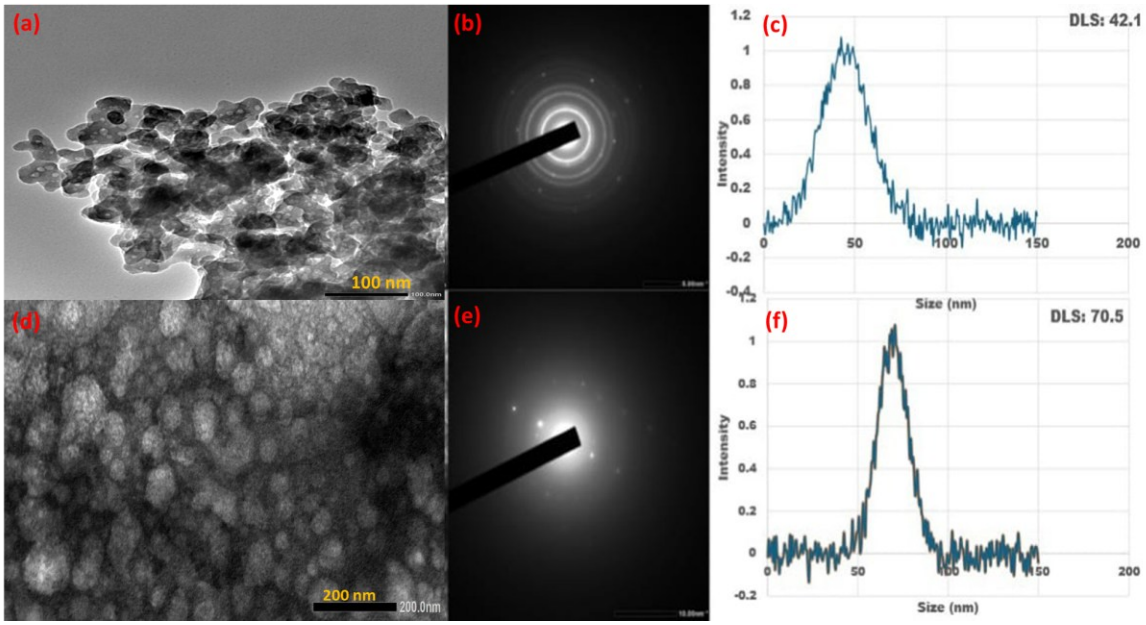

Fig. 1. (a, d) HR-TEM images, (b, e) SAED pattern, and (c, f) DLS analysis of CeO_2 and CeO_2/CuO NPs, respectively

Zeta Potential, XRD, and FTIR Analysis of NPs

Zeta potential data were used to determine each sample's isoelectric point (IEP). The IEP values for synthesized CeO_2 and CeO_2/CuO NPs both appeared at -31.5 mV (Figs. 2a, 2b). XRD was used to examine the structural properties of CeO_2 and CeO_2/CuO NPs (Figs. 2c, 2d, respectively). CeO_2 NPs were found to have diffraction peaks at 2θ = 29.4 (111) 31.9 (200), 47.8 (220), 55.6 (311), 59.8 (222) and 68.7 (400). CuO NPs' crystalline phases, on the other hand, exhibited diffraction peaks at 2θ = 35.9 (002), 38.8 (111), 47.3 (200), 57.71(021), and 68.5 (220). These findings provide more evidence of the material's cubic and monoclinic structures of CeO_2 and CuO, respectively. The indexed crystalline planes agreed well with the standard values of JCPDS card Nos. (34–0394) and (48–1548) of CeO_2 and CeO NPs, respectively (Salih *et al*. 2024).

Scherrer's equation was used to calculate the crystallite size based on X-ray data. According to the Scherer equation, the crystallite sizes of CeO_2 and CeO_2/CuO NPs were 20.5 and 26.8 nm, respectively. The following were calculated: d-spacing (dhkl=λ/(2sin θ), micro-strain (ε=β/4tan θ), and dislocation density (δ=1/D^2) (Tables 1 and 2).

Table 1. XRD Parameters for CeO_2 NPs

2θ	FWHM(β)	Size nm	Dislocation density (δ)	Micro-Strain (ε)	d-Spacing
29.4	0.17	47.71	0.43	2.85	1.56
31.9	0.55	14.88	4.51	8.46	1.45
47.8	1.78	4.85	42.37	17.59	1.03
55.6	0.35	25.34	1.55	2.92	0.93
59.8	0.79	11.49	7.57	6.04	0.89
68.7	0.51	18.57	2.89	3.30	0.82
Average	0.69	20.47	9.89	6.86	1.11

Table 2. XRD Parameters for CeO_2 /CuO NPs

2θ	FWHM (β)	Size (nm)	Dislocation density (δ)	Micro-Strain (ε)	d-Spacing
28.9	0.45	18.14	3.03	7.65	1.59
35.9	0.35	23.51	1.80	4.78	1.31
38.8	0.78	10.67	8.77	9.77	1.22
47.3	0.12	86.72	0.13	0.99	1.04
48.7	0.37	21.92	2.08	3.83	1.02
55.9	1.51	5.92	28.49	12.48	0.93
57.7	0.32	28.25	1.25	2.54	0.91
68.5	0.49	19.61	2.59	3.14	0.82
Average	0.55	26.84	6.02	5.65	1.10

The FTIR spectra of the CeO_2 NPs and CeO_2/CuO NPs were also examined in order to pinpoint the precise functional groups that caused the reduction of the produced NPs. In the FTIR, the CeO_2/CuO NPs showed the most notable peaks at 3450, 2361, 1551, 1412, 1020, 930, 663, and 510 cm^{-1}, while the CeO_2 NPs showed the most prominent peaks at 3426, 2434, 2090, 1785, 1582, 1380, 1059, and 828 cm^{-1}. The large peaks at (3426, 3450 cm^{-1}) in Figs. (2e, 2f) were caused by the O-H stretching vibration caused by the alcoholic group. The absorbance peak at 1582 cm^{-1} was caused by the scissor bending mode of the connected water (Kumar *et al*. 2010). At 1020 cm^{-1}, the stretching vibration of C-O was observed (Farahmandjou *et al*. 2016). The absorbance peaks at 930, 828, and 510 cm^{-1} were caused by the metal-oxygen bonds, or Ce-O and Cu-O bonds, according to Kumar *et al*. (2010) and Pujar *et al*. (2018).

The appearance of peaks for the metal-oxygen link indicated the creation of copper oxide and cerium oxide nanoparticles. The FTIR data indicated the presence of biomolecules in the plant extract that were responsible for the synthesis and production of the CeO_2 NPs and CeO_2/CuO NPs by showing the adsorption of different functional groups on the surface of the NPs (Arunachalam *et al*. 2017; Pisal *et al*. 2019).

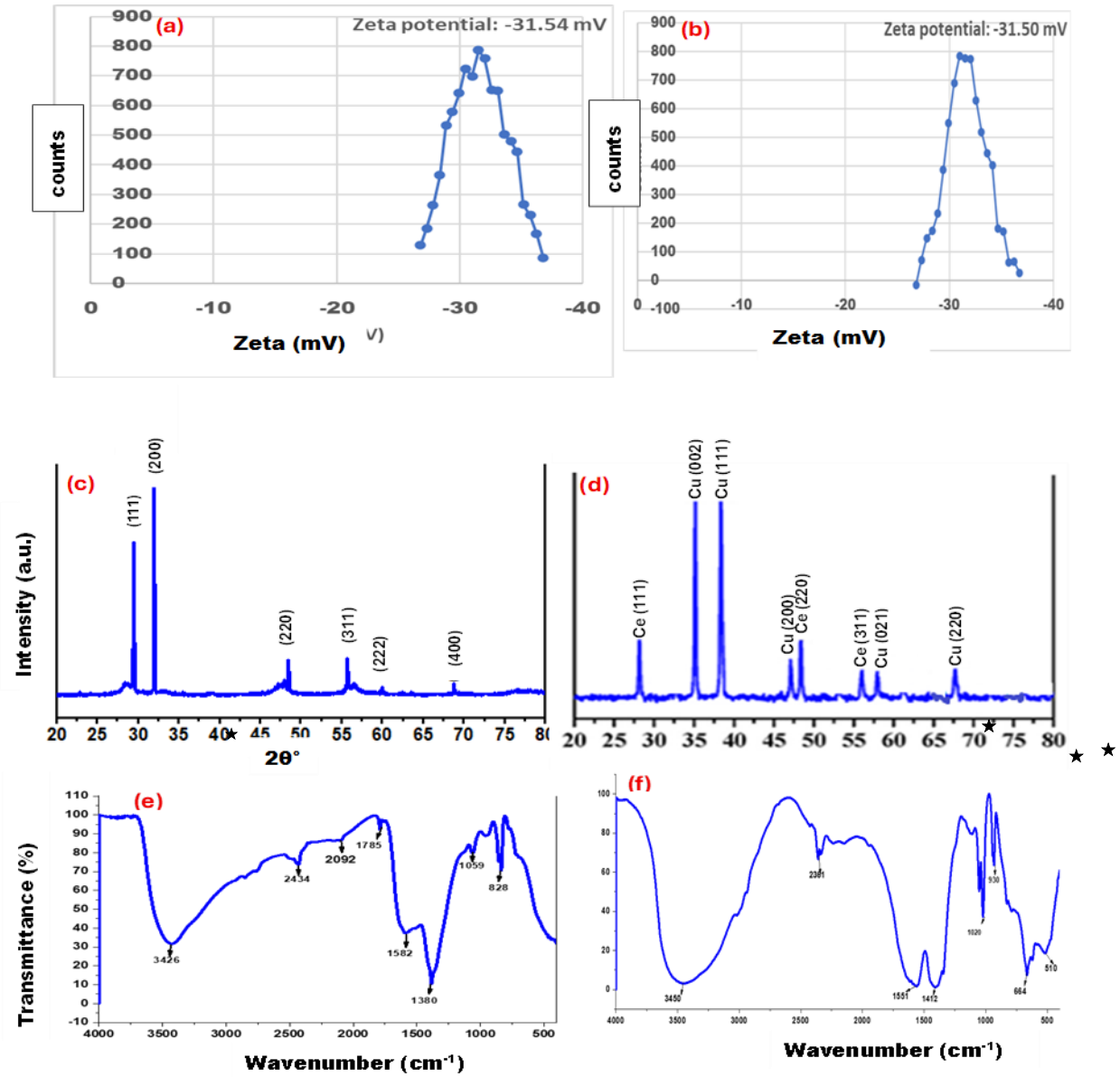

Fig. 2. Zeta potential (a,b), XRD (c,d), and FTIR (e,f) analysis of CeO_2 NPs and CeO_2/CuO nanocomposite, respectively

Anti-microbial Activity of CeO_2/CuO Nanocomposite NPs and CeO_2 NPs

A panel of bacteria was employed to evaluate the antimicrobial activity of CeO_2/CuO nanocomposite in comparison to CeO_2 NPs and conventional antibiotic/antifungal drugs (Table 3). In comparison to CeO_2 NPs (24 ± 1.0 mm) and the control antibiotic (22 ± 0.1 mm), the CeO_2/CuO nanocomposite demonstrated the best inhibitory activity versus *B. subtilis*, generating an inhibition zone of 26 ± 0.4 mm. The MBC values of both nanomaterials were 62.5 µg/mL, and they both showed the identical MIC value of 31.2 µg/mL. The CeO_2 NPs demonstrated a marginally greater inhibitory zone (18 ± 0.5 mm) against *S. aureus* than the nanocomposite (16 ± 1 mm), which was similar to the control antibiotic (18 ± 0.3 mm). Despite both nanomaterials having the same MIC 62.5 µg/mL, the MBC of the nanocomposite was greater (125 µg/mL) compared to that of CeO_2 nanoparticles (62.5 µg/mL), indicating a diminished bactericidal effectiveness

in this instance. For *K. pneumoniae*, both nanomaterials displayed nearly equivalent inhibition zones (19 ± 0.5 and 19 ± 0.8 mm, respectively), which were also similar to that of the antibiotic (18 ± 0.2 mm). The MIC and MBC values were consistent for both nanomaterials at 31.2 µg/mL. In a similar manner, *S. typhi* was inhibited to a comparable degree by the nanocomposite (16 ± 0.1 mm), CeO_2 NPs (15 ± 0.9 mm), and the antibiotic (16 ± 0.1 mm), with both nanomaterials demonstrating identical MIC (31.25 µg/mL) and MBC (62.5 µg/mL). A significant antifungal effect was noted against *C. albicans*, with the CeO_2/CuO nanocomposite demonstrating the largest inhibition zone of 28 ± 0.8 mm, surpassing both CeO_2 NPs at 24 ± 1.0 mm and the control antifungal at 21 ± 0.3 mm. Both nanomaterials exhibited MIC of 15.6 µg/mL and a MFC of 31.2 µg/mL, reflecting robust fungistatic and fungicidal properties. Conversely, no inhibitory effect was detected for either nanomaterial against *A. niger*, while the control antifungal showed a clear inhibition zone of 38 ± 0.8 mm. In general, these results suggest that the CeO_2/CuO nanocomposite has superior antimicrobial efficacy compared to CeO_2 NPs alone, especially against *B. subtilis* and *C. albicans*, whereas both materials were ineffective against *A. niger*. This is likely due to the thicker, multi-layered hyphal cell walls and the filamentous growth pattern, which limit nanoparticle penetration and reduce local nanoparticle concentration per active site. Additionally, slower metabolism in filamentous fungi may reduce susceptibility to oxidative stress induced by the nanoparticles.

Table 4 presents the killing kinetics of *B. subtilis*, *S. aureus*, *K. pneumoniae*, and *S. typhi* when subjected to treatment with CeO_2/CuO nanocomposite NPs in comparison to CeO_2 NPs alone. Bacterial counts, represented as colony-forming units (CFU), were tracked at various exposure intervals (0 to 180 min). For the CeO_2/CuO nanocomposite, all four bacterial species exhibited a gradual reduction in CFU as exposure time increased. At the starting point (0 min), bacterial counts ranged from 22×10^5 to 34×10^5 CFU. Following 30 min of treatment, CFU values significantly decreased, with *B. subtilis* dropping to 1.1×10^5 CFU, *K. pneumoniae* to 4.5×10^4 CFU, *S. aureus* to 2.7×10^5 CFU, and *S. typhi* to 2.3×10^5 CFU. By the 120-min mark, CFU counts had significantly fallen, reaching 6.4×10^2 for *B. subtilis*, 4.4×10^2 for *K. pneumoniae*, 1.2×10^3 for *S. aureus*, and 3.7×10^2 for *S. typhi*. Complete bacterial elimination was noted at 180 minutes for *B. subtilis* and *K. pneumoniae*, while only a few survivors remained in *S. aureus* (14 CFU) and *S. typhi* (24 CFU). When treated solely with CeO_2 NPs, a comparable yet slightly slower trend in bacterial reduction was noted. After 30 min, reductions were observed, although they were less significant than those seen with the nanocomposite, with *B. subtilis* at 8.7×10^4 CFU, *K. pneumoniae* at 1.3×10^5 CFU, *S. aureus* at 1.1×10^5 CFU, and *S. typhi* at 1.7×10^5 CFU. At the 120-min mark, the counts for *B. subtilis* and *S. aureus* decreased to 1.7×10^2 and 1.3×10^2 CFU, respectively, while *K. pneumoniae* and *S. typhi* remained elevated at 3.6×10^2 and 1.9×10^3 CFU. By 180 min, *B. subtilis*, *K. pneumoniae*, and *S. aureus* were entirely eradicated, whereas a small quantity of *S. typhi* cells (37 CFU) persisted.

Table 3. Anti-microbial Activity of CeO_2/CuO Nanocomposite NPs and CeO_2 NPs with Standard Antibiotic/Antifungal

Tested Bacteria/Fungi	Inhibition Zones (mm)			MIC (µg/mL)		MBC/MFC (µg/mL)	
	CeO_2/CuO Nanocomposite	CeO_2 NPs	Control Antibiotic	CeO_2/CuO Nanocomposite	CeO_2 NPs	CeO_2/CuO nanocomposite	CeO_2 NPs
B. subtilis	26±0.4	24±1.0	22±0.1	31.25	31.25	62.5	62.5
S. aureus	16±1	18±0.5	18±0.3	62.5	62.5	125	62.5
K. pneumonia	19±0.5	19±0.8	18±0.2	31.25	31.25	31.25	31.25
S. typhi	16±0.1	15±0.9	16±0.1	31.25	31.25	62.5	62.5
C. albicans	28±0.8	24±1.0	21±0.3	15.62	15.62	31.25	31.25
A. niger	NA	NA	38±0.8	--	--	--	--

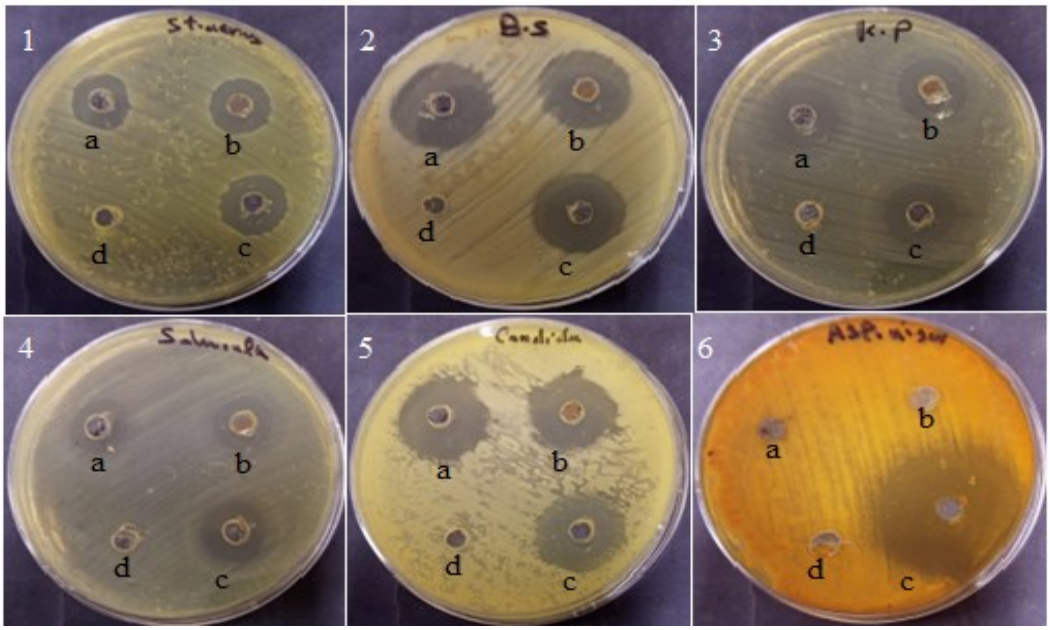

Fig. 3. Antimicrobial activity of CeO_2/CuO nanocomposite and CeO_2 NPs against (1) *Staphylococcus aureus*, (2) *Bacillus subtilis*, (3) *Klebsiella pneumoniae*, (4) *Salmonella typhi*, (5) *Candida albicans*, and (6) *Aspergillus niger*. (a) CeO_2/CuO nanocomposite (b) CeO_2 NPs, (c) standard antibiotic/antifungal, and (d) control (DMSO). Clear inhibition zones indicate the sensitivity of each microorganism to the tested nanoparticles.

Overall, these findings suggest that both the CeO_2/CuO nanocomposite and CeO_2 NPs exhibit significant time-dependent bactericidal properties, with the nanocomposite achieving a quicker and more effective reduction, especially against *B. subtilis* and *K. pneumoniae*. Previous studies have demonstrated that Cu-doped CeO_2 NPs possess notable antimicrobial activity, with MIC values varying according to the tested strain: 16 mg/L against *Enterococcus hirae* and *E. faecalis*, 32 mg/L against *S. aureus*, 64 mg/L against *Escherichia coli*, 128 mg/L against *Pseudomonas aeruginosa* and *Legionella pneumophila* subsp. *pneumophila*, and 256 mg/L against *Candida tropicalis* and *C. albicans* (Şener *et al*. 2017). Although the exact antibacterial mechanism remains to be fully clarified, it has been suggested that the negatively charged bacterial cell walls may interact electrostatically with the positively charged Cu@nano-CeO_2, thereby facilitating their attachment and

subsequent entry into the cells. This interaction may lead to changes in membrane fluidity and reduced cell viability, as observed in *E. coli* following 2 h of exposure (Şener *et al*. 2017). Nanoparticles–cell interactions are thought to involve electrostatic forces, van der Waals interactions, hydrophobic effects, and receptor–ligand binding, all of which can compromise the integrity of the bacterial membrane. Furthermore, Cu@nano-CeO_2 has been reported to strongly associate with membrane lipids, enabling penetration into the bilayer and promoting oxidation of phospholipids by Ce^{4+} ions, ultimately resulting in membrane instability and decreased fluidity (Zhuo *et al*. 2021). In agreement with these earlier findings, these results confirm that the CeO_2/CuO nanocomposite exhibits a potent inhibitory effect against pathogenic bacteria, supporting its potential as a broad-spectrum antimicrobial agent.

Table 4. Effect of Different Killing Kinetic Times of *B. subtilis*, *S. aureus*, *K. pneumonia,* and *S. typhi,* Treated by CeO_2/CuO Nanocomposite and CeO_2 NPs

Killing Kinetic Time (min)	CFU Treated by CeO_2/CuO Nanocomposite NPs			
	B. subtilis	*K. pneumoniae*	*S. aureus*	*S. typhi*
0	29×10^5 ±1.0	22×10^5±2.0	31×10^5±2.0	34×10^5±1
30	110×10^4±3.0	45×10^4±1	272×10^4±1	231×10^4±2
60	33×10^3± 2	72×10^3±2.0	116×10^3±2	181×10^3±2.0
120	64×10^2 ±1.0	44^*10^2±2.0	120×10^2 ±2	37×10^2 ±3.0
150	110±1.0	22	245	293
180	0	0	14	24
Killing Kinetic Time (min)	CFU Treated by CeO_2 NPs			
	B. subtilis	*K. pneumoniae*	*S. aureus*	*S. typhi*
	29×10^5 ±1.0	22×10^5±2.0	31×10^5±2.0	34×10^5±1
30	87×10^4±2.0	133×10^4±2.0	113×10^4±1	174×10^4±2
60	24×10^3± 1.0	94×10^3±2.0	38×10^3±2.0	32×10^3±1
120	17×10^2 ±2.0	36×10^2±2.0	13×10^2±2.0	194×10^2±1
150	31	39	5	289
180	0	0	0	37

CONCLUSIONS

1. In this study CeO_2 NPs and CeO_2/CuO nanocomposite particles were prepared from the medicinally significant plant *Ficus religiosa* and its potential as an antibacterial agent was investigated.
2. XRD, FTIR, SAED, zeta potential, DLS, and TEM analyses were used to characterize the prepared nanoparticles. Based on the XRD data, the CeO_2 and CeO_2/CuO NPs' diffraction peaks showed cubic and monoclinic structures, respectively, with average crystallite sizes of 20.5 and 26.8 nm, respectively. The mean sizes of the CeO_2 and CeO_2/CuO NPs (39.8 and 66.5 nm, respectively) are consistent with very little agglomeration, according to TEM analyses.
3. Ce-O, Cu-O bonds, and other bonds were identified using the CeO_2 and CeO_2/CuO NPs' FT-IR spectra.

4. Wider inhibitory zones, low MIC/MBC/MFC numbers, and quick bacterial death after 180 minutes demonstrated that the CeO_2/CuO nanocomposite had more potent and extensive antibacterial activity than pure CeO_2 NPs. Its potency as an antibacterial and antifungal agent was demonstrated by its strong action against *Bacillus subtilis*, *Staphylococcus aureus*, *Klebsiella pneumoniae*, *Salmonella typhi*, and *Candida albicans*. But the absence of action against *Aspergillus niger* suggests a process of selection. According to these results, CeO_2/CuO nanocomposites may be a good option for creating novel antimicrobial formulations to fight microorganisms with resistance.

Funding

This work was funded by the Deanship of Graduate Studies and Scientific Research at Jouf University under grant No. (DGSSR-2025-FC-01007).

REFERENCES CITED

Abbasi, N., Homayouni Tabrizi, M., Ardalan, T., & Roumi, S. (2022). "Cerium oxide nanoparticles-loaded on chitosan for the investigation of anticancer properties," *Materials Technology*, *37*(10), 1439-1449. https://doi.org/10.1080/10667857.2021.1954279

Abdelghany, T. M. (2013). "*Stachybotrys chartarum*: A novel biological agent for the extracellular synthesis of silver nanoparticles and their antimicrobial activity," *Indonesian Journal of Biotechnology* 18(2), 75-82. https://doi.org/10.22146/ijbiotech.7871

Abdelghany, T. M., Al-Rajhi, A. M. H., Al Abboud, M. A., Alawlaqi, M. M., Magdah, A. G., Helmy, E. A. M., and Mabrouk, A. S. (2018). "Recent advances in green synthesis of silver nanoparticles and their applications: About future directions. A review," *BioNanoScience* 8, 5-16. https://doi.org/10.1007/s12668-017-0413-3

Al Abboud, M. A., Mashraqi, A., Qanash, H., Gattan, H. S., Felemban, H. R., Alkorbi, F., Alawlaqi, M. M., Abdelghany, T. M., Moawad, H. (2024). "Green biosynthesis of bimetallic ZnO@AuNPs with its formulation into cellulose derivative: Biological and environmental applications," *Bioresour. Bioprocess* 11(1), 60. https://doi.org/10.1186/s40643-024-00759-3

Al-Attar, H. M., Mohammad, M. H., Majeed, A. M., Hussein, H. T., and Ahmed, A. A. (2025). "Investigating the anticancer activity of cerium nanoparticles decorated on GO produced by green methods against cancerous cell lines," *Asian Pacific Journal of Cancer Prevention: APJCP* 26(2), 541. https://doi.org/10.31557/APJCP.2025.26.2.541

Alghonaim, M. I., Alsalamah, S. A., Ali, Y., and Abdelghany, T. M. (2024). "Green mediator for selenium nanoparticles synthesis with antimicrobial activity and plant biostimulant properties under heavy metal stress," *BioResources* 19(1), 898-916. https://doi.org/10.15376/biores.19.1.898-916

Alghonaim, M. I., Alsalamah, S. A., Mohammad, A. M., and Abdelghany, T. M. (2025). "Green synthesis of bimetallic Se@TiO_2 NPs and their formulation into biopolymers and their utilization as antimicrobial, anti-diabetic, antioxidant, and healing agent *in vitro*," *Biomass Conversion and Biorefinery* 15, 6767-6779. https://doi.org/10.1007/s13399-024-05451-2

Al-Rajhi, A. M. H., Yahya, R., Bakri, M. M., Yahya, R., and Abdelghany, T. M. (2022b). "In situ green synthesis of Cu-doped ZnO-based polymer nanocomposite with antimicrobial, antioxidant, and anti-inflammatory activities," *Applied Biological Chemistry* 65, artilce 35. https://doi.org/10.1186/s13765-022-00702-0

Al-Rajhi, A. M., Salem, S. S., Alharbi, A. A., and Abdelghany, T. M. (2022a). "Ecofriendly synthesis of silver nanoparticles using Kei-apple (*Dovyalis caffra*) fruit and their efficacy against cancer cells and clinical pathogenic microorganisms," *Arabian Journal of Chemistry* 15(7), article 103927. https://doi.org/10.1016/j.arabjc

Amin, M. A. A., Abu-Elsaoud, A. M., Nowwar, A. I., Abdelwahab, A. T., Awad, M. A., Hassan, S. E. D., and Elkelish, A. (2024). "Green synthesis of magnesium oxide nanoparticles using endophytic fungal strain to improve the growth, metabolic activities, yield traits, and phenolic compounds content of *Nigella sativa* L.," *Green Processing and Synthesis* 13(1), article 20230215. https://doi.org/10.1515/gps-2023-0215

Amin, M. A., Algamdi, N. A., Waznah, M. S., Bukhari, D. A., Alsharif, S. M., Alkhayri, F., Abdel-Nasser, M., and Fouda, A. (2025). "An insight into antimicrobial, antioxidant, anticancer, and antidiabetic activities of trimetallic Se/ZnO/CuO nanoalloys fabricated by aqueous extract of *Nitraria retusa*," *Journal of Cluster Science* 36(1), 1-15. https://doi.org/10.1007/s10876-024-02742-6

Amiri, M. S., Mohammadzadeh, V., Yazdi, M. E. T., Barani, M., Rahdar, A., and Kyzas, G. Z. (2021). "Plant-based gums and mucilages applications in pharmacology and nanomedicine: A review," *Molecules* 26(6), article 1770. https://doi.org/10.3390/molecules26061770

Arunachalam, T., Karpagasundaram, M., and Rajarathinam, N. (2017). "Ultrasound-assisted green synthesis of cerium oxide nanoparticles using *Prosopis juliflora* leaf extract and their structural, optical and antibacterial properties," *Materials Science-Poland* 35(4), 791-798. https://doi.org/10.1515/msp-2017-0104

Aseyd Nezhad, S., Es-haghi, A., and Tabrizi, M. H. (2020). "Green synthesis of cerium oxide nanoparticles using *Origanum majorana* L. leaf extract, its characterization and biological activities," *Applied Organometallic Chemistry* 34(2), article e5314. https://doi.org/10.1002/aoc.5314

Ashna, M., Es-Haghi, A., Karimi Noghondar, M., Al Amara, D., and Yazdi, M. E. T. (2022). "Greener synthesis of cerium oxide nanoemulsion using pollen grains of *Brassica napus* and evaluation of its antitumour and cytotoxicity properties," *Materials Technology* 37(8), 525-532. https://doi.org/10.1080/10667857.2020.1863558

Butt, A., Sarfraz Ali, J., Sajjad, A., Naz, S., and Zia, M. (2022). "Biogenic synthesis of cerium oxide nanoparticles using petals of *Cassia glauca* and evaluation of antimicrobial, enzyme inhibition, antioxidant, and nanozyme activities," *Biochemical Systematics and Ecology* 104, article 104462. https://doi.org/10.1016/j.bse.2022.104462

Farahmandjou, M., Zarinkamar, M., and Firoozabadi, T. P. (2016). "Synthesis of cerium oxide (CeO_2) nanoparticles using simple co-precipitation method," *Revista Mexicana de Física* 62(5), 496-499.

Fauzia, Khan, M. A., and Chaman, M. (2024). "Antibacterial and sunlight-driven photocatalytic activity of graphene oxide conjugated CeO_2 nanoparticles," *Scientific Reports* 14, article 6606. https://doi.org/10.1038/s41598-024-54905-0

Jelonek, K., Zajdel, A., Wilczok, A., Latocha, M., Musiał-Kulik, M., Foryś, A., and Kasperczyk, J. (2019). "Dual-targeted biodegradable micelles for anticancer drug delivery," *Materials Letters* 241, 187-189. https://doi.org/10.1016/j.matlet.2019.01.081

Kumar, E., Selvarajan, P., and Balasubramanian, K. (2010). "Preparation and studies of cerium dioxide (CeO_2) nanoparticles by microwave-assisted solution method," *Recent Research in Science and Technology* 2(4), 37-41.

Lu, H., Wan, L., Li, X., Zhang, M., Shakoor, A., Li, W., & Zhang, X. (2022). "Combined synthesis of cerium oxide particles for effective anti-bacterial and anti-cancer nanotherapeutics," *International journal of nanomedicine*, *17*, 5733. https://doi.org/10.2147/IJN.S379689

Nadeem, M., Khan, R., Afridi, K., Nadhman, A., Ullah, S., Faisal, S., Mabood, Z. U., Hano, C., and Abbasi, B. H. (2020). "Green synthesis of cerium oxide nanoparticles (CeO_2 NPs) and their antimicrobial applications: A review," *International Journal of Nanomedicine*, 5951-5961. https://doi.org/10.2147/IJN.S255784

Naz, S., Kazmi, S. T. B., and Zia, M. (2019). "CeO_2 nanoparticles synthesized through green chemistry are biocompatible: *In vitro* and *in vivo* assessment," *Journal of Biochemical and Molecular Toxicology* 33(5), article e22291. https://doi.org/10.1002/jbt.22291

Pisal, V., Wakchaure, P., and Patil, N. (2019). "Green synthesized CeO_2 quantum dots: A study of its antimicrobial potential," *Materials Research Express* 6(11), article 115409. https://doi.org/10.1088/2053-1591/ab4fa5

Pujar, M. S., Hunagund, S. M., Desai, V. R., Patil, S., and Sidarai, A. H. (2018). "One-step synthesis and characterization of cerium oxide nanoparticles in ambient temperature *via* co-precipitation method," *AIP Conference Proceedings* 1942(1), article 050026. https://doi.org/10.1063/1.5028657

Sadidi, H., Hooshmand, S., Ahmadabadi, A., Hoseini, S. J., Baino, F., Vatanpour, M., and Kargozar, S. (2020). "Cerium oxide nanoparticles (nanoceria): Hopes in soft tissue engineering," *Molecules* 25(19), article 4559. https://doi.org/10.3390/molecules25194559

Salih, W. M., Sabah, R., Kadhim, D. A., Kadhum, H. A., and Abid, M. A. (2024). "Green synthesis of (CeO_2)-(CuO) nanocomposite, analytical study, and investigation of their anticancer activity against Saos-2 osteosarcoma cell lines," *Inorganic Chemistry Communications* 159, article 111730. https://doi.org/10.1016/j.inoche.2023.111730

Sarita Rai, Preeti Gupta, and Singh, N. B. (2024). "Biomedical applications of green synthesized cerium oxide nanoparticles," *Materials Research Foundations* 169, 173-196. https://doi.org/10.21741/9781644903261-7

Selim, S., Abdelghany, T. M., Almuhayawi, M. S., Nagshabandi, M. K., Tarabulsi, M. K., Elamir, M. Y. M., Alharbi, A. A., and Al Jaouni, S. K. (2025a). "Biosynthesis and activity of Zn–MnO nanocomposite *in vitro* with molecular docking studies against multidrug resistance bacteria and inflammatory activators," *Scientific Reports* 15, article 2032. https://doi.org/10.1038/s41598-024-85005-8

Selim, S., Saddiq, A. A., Ashy, R. A., Baghdadi, A. M., Alzahrani, A. J., Mostafa, E. M., Al Jaouni, S. K., Elamir, M. Y. M., Amin, M. A., Salah, A. M., and Hagagy, N. (2025b). "Bimetallic selenium/zinc oxide nanoparticles: Biological activity and plant biostimulant properties," *AMB Express* 15(1), 1–11. https://doi.org/10.1186/s13568-024-01808-y

Selim, S., Alruwaili, Y., Ejaz, H., Abdalla, A. E., Almuhayawi, M. S., Nagshabandi, M. K., and Abdelghany, T. M. (2024). "Estimation and action mechanisms of cinnamon bark via oxidative enzymes and ultrastructures as antimicrobial, anti-biofilm, antioxidant, anti-diabetic, and anticancer agents," *BioResources* 19(4), 7019-7041. https://doi.org/10.15376/biores.19.4.7019-7041

Şener, L., Özdemir, S., Yalçın, M. S., Gülcan, M., and Dizge, N. (2024). "Antibacterial activity of copper-decorated CeO_2 nanoparticles and preparation of antifouling polyethersulfone surface," *Heliyon* 10(23), article e40818. https://doi.org/10.1016/j.heliyon.2024.e40818

Soliman, M. K., Amin, M. A. A., Nowwar, A. I., Hendy, M. H., and Salem, S. S. (2024). "Green synthesis of selenium nanoparticles from *Cassia javanica* flowers extract and their medical and agricultural applications," *Scientific Reports* 14(1), article 26775. https://doi.org/10.1038/s41598-024-77353-2

Valsaraj, P. V., and Divyarthana. (2019). "Structural, optical, and antimicrobial properties of green synthesized cerium oxide nanoparticles," *AIP Conference Proceedings* 2162(1), article 020022. https://doi.org/10.1063/1.5130232

Zhuo, M., Ma, J., and Quan, X. (2021). "Cytotoxicity of functionalized CeO_2 nanoparticles towards *Escherichia coli* and adaptive response of membrane properties," *Chemosphere* 281, article 130865. https://doi.org/10.1016/j.chemosphere.2021.130865

Article submitted: October 4, 2025; Peer review completed: December 12, 2025; Revised version received and accepted: December 15, 2025; Published: December 21, 2025.
DOI: 10.15376/biores.21.1.1224-1237